Nuclear Magnetic Resonance Structure of a Prototype Lin12-Notch Repeat Module from Human Notch1[†]

Didem Vardar, Christopher L. North, Cheryll Sanchez-Irizarry, Jon C. Aster, and Stephen C. Blacklow*

Department of Pathology, Brigham and Women's Hospital and Harvard Medical School, 75 Francis Street, Boston, Massachusetts 02115

Received January 28, 2003; Revised Manuscript Received April 18, 2003

ABSTRACT: Notch1 is a member of a conserved family of large modular heterodimeric type 1 transmembrane receptors that control differentiation in multicellular animals. Receptor maturation is accompanied by a furin-dependent cleavage that converts the Notch1 precursor polypeptide into a heterodimer consisting of an extracellular ligand-binding subunit (NEC) and a transmembrane signaling subunit (NTM). Binding of a physiologic ligand to NEC induces signaling by triggering additional proteolytic cleavages in NTM, which allow its intracellular region to translocate to the nucleus where it participates in a transcriptional activation complex. In the absence of ligand, the three conserved LNR modules of the NEC subunit participate in maintaining the receptor in its resting conformation. Here, we report the solution structure of the first LNR module (LNR_A) of human Notch1, and identify residues of LNR_A perturbed by the presence of the adjacent module LNR_B. LNR_A is held together by a unique arrangement of three disulfide bonds and a single bound Ca^{2+} ion, and adopts a novel fold that falls in the general class of irregular disulfide-bonded structures. Residues perturbed by the presence of the adjacent LNR_B module are predominantly hydrophobic, and lie on one face of the module. These studies represent an initial step toward understanding the structural interrelationships among the three contiguous LNR modules required for proper regulation of Notch signaling.

Drosophila Notch and its homologues in other multicellular animals are modular single-pass transmembrane receptors that participate in a highly conserved signal transduction pathway. Notch signals are broadly important in regulating cell growth, differentiation, and survival in a variety of different contexts, facilitating development and maintenance of many normal tissues and cell types (*1*). When Notch signaling is not properly regulated, a variety of phenotypes may appear, including some forms of human disease. For example, signals transduced by Notch1, one of four Notch proteins in mammals, orchesterate normal differentiation of T lymphocytes (*2*), but constitutive upregulation of Notch1 signaling causes sporadic human and experimental murine T-cell acute leukemias (*3*−*5*).

Human Notch1 (hNotch1) is initially synthesized as a 350 kDa precursor glycoprotein, which is processed at site S1 by a furin-like protease during transport to the cell surface to produce a heterodimer consisting of noncovalently associated extracellular (NEC) and transmembrane (NTM) subunits (Figure 1). Binding of a DSL ligand (Delta, Serrate, or LAG-2) to NEC initiates two successive proteolytic cleavages that occur through a process termed regulated intramembrane proteolysis (*6*). The first cleavage by a metalloprotease at site S2 renders NTM susceptible to the second essential cleavage at site S3 close to the inner leaflet of the plasma membrane. Site S3 cleavage, which is catalyzed by a multiprotein complex containing presenilin and nicastrin (*7*−*10*), liberates the intracellular portion of NTM from the membrane, allowing it to translocate to the nucleus and activate transcription of target genes (*11, 12*).

Notch proteins exhibit a highly conserved modular architecture (Figure 1), in which distinct repeated structural units are associated with different functional roles in the intact receptor. The ligand-binding site of hNotch1 lies within the N-terminal series of 36 EGF-like modules, which constitute the bulk of the NEC subunit. The EGF repeats are followed by a negative-regulatory region (NRR) that is responsible for maintaining the receptor in a resting state prior to ligand binding. This NRR includes three Notch-specific Lin12-Notch repeats (LNRs) and an additional 103-residue sequence up to the furin cleavage site (S1) that defines the C-terminal end of NEC. The NTM subunit has a 69-residue extracellular region (NTM-E, which harbors the S2 cleavage site), a transmembrane segment (which contains the S3 cleavage site), and a large intracellular part that includes a RAM domain, ankyrin repeats, a transactivation domain, and a carboxy-terminal PEST sequence (Figure 1).

To date, LNR modules have been identified in only Notch receptors. Each 35−40-residue LNR module contains three disulfide bonds and a group of conserved acidic and polar residues predicted to coordinate a calcium (Ca^{2+}) ion (*13*). Alignment of the LNRs in the sequence database reveals that

[†] Supported by NIH Grants R01-CA92433 (S.C.B.) and R01-CA82308 (J.C.A.). S.C.B. is a Pew Scholar in the Biomedical Sciences and an Established Investigator of the American Heart Association.

* To whom correspondence should be addressed. Telephone: (617) 732-5799. Fax: (617) 264-5296. E-mail: sblacklow@rics.bwh.harvard.edu.

10.1021/bi034156y CCC: $25.00
Published on Web 05/20/2003

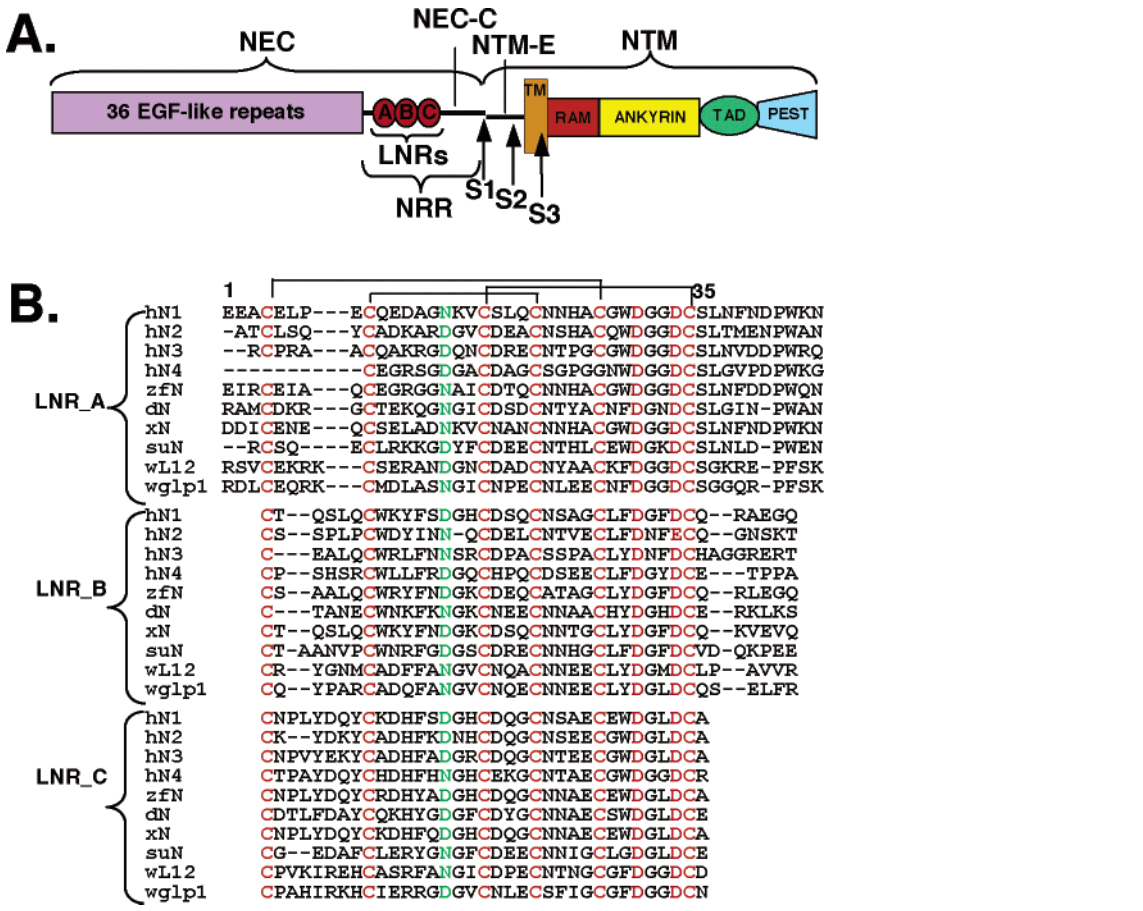

FIGURE 1: (A) Domain organization of human Notch1 (hNotch1). NEC consists of 36 epidermal growth factor (EGF)-like repeats and a negative-regulatory region (NRR) containing the three family specific LIN12/Notch repeats (LNRs) and a 100-residue C-terminal tail (NEC-C). NTM contains a short extracellular region (NTM-E), a transmembrane segment, a RAM domain, seven ankyrin repeats, a transactivation domain (TAD), and a carboxy-terminal PEST sequence. S1−S3 are furin, metalloprotease, and presenilin-dependent cleavage sites, respectively. (B) Sequence alignment of the three LNRs from different Notch proteins: h, human; zfN, zebrafish; d, *Drosophila*; x, *Xenopus*; su, sea urchin; w, *Caenorhabditis elegans*. Conserved cysteine residues (orange) and Ca^{2+}-coordinating residues (D30/D33 red; N15, green) from hNotch1 LNR_A are highlighted.

these modules are always found *en bloc* as a group of three and are the most highly conserved part of the NEC subunit. This high degree of sequence conservation likely reflects the functional importance of the LNRs in maintaining the receptor in its resting conformation prior to ligand binding. Assignment of this functional role to the LNRs is supported by observations showing that point mutations in the LNRs of the worm Notch receptor LIN12 result in gain-of-function phenotypes (*14*), and that deletions removing the LNRs lead to activation of Notch signaling in reporter assays (ref *15* and unpublished observations of J. C. Aster).

Because the LNRs participate in control of Notch activation and represent highly conserved unique structural modules of the Notch receptor ectodomain, we determined the structure of a prototype LNR module from hNotch1 (LNR_A) by NMR. This structure provides the first atomic-resolution information about any Notch LNR repeat and defines the distinct features of this novel protein module. By further identifying sites of perturbation resulting from the added presence of the adjacent LNR_B module, we also take an initial step toward understanding the structural interrelationships among the three contiguous LNR modules within the Notch NRR, a key region of the receptor required for proper regulation of signaling.

MATERIALS AND METHODS

Protein Expression and Purification. LNR_A (hNotch1 residues 1446−1480) was expressed, purified, and refolded essentially as described previously (*13*). Uniformly ^{15}N-labeled proteins were purified from cells grown in M9T minimal medium with $^{15}NH_4Cl$ as the sole source of nitrogen, and [^{13}C]glucose was added to produce the doubly ^{15}N- and ^{13}C-labeled protein. Purified proteins were lyophilized and stored at 4 °C until they were used. LNR_B (residues 1481−1528) and LNR_AB (residues 1446−1528) were purified using the same strategy and stored in the same way.

Calorimetry Experiments. For isothermal titration calorimetry (ITC) experiments, a stock solution of 1 mM $CaCl_2$ was added in 7.5 μL increments to a 100 μM LNR_A solution in 50 mM PIPES (pH 6.0) buffer at room temperature. Protein concentrations were determined using the UV absorbance of LNR_A at 280 nm. The raw data were baseline corrected, and the binding curve was plotted using Origin 5.0. The dissociation constant was extracted from curve fitting the data to a one-site binding model using the ITC module of the Origin software package.

NMR Spectrometry. Spectra were acquired on a Varian Unity 400 MHz, Bruker 500 MHz, or Bruker 600 MHz spectrometer equipped with either a triple-resonance cryo-

probe or a regular probe. All spectrometers are equipped with pulsed field gradient units and with actively shielded *Z*-gradients. Spectra were acquired using standard procedures (*16*), processed on Silicon Graphics workstations with Felix 97 software (MSI) and NmrPIPE (*17*), and analyzed using NmrView (*18*). Under the conditions used for the NMR experiments (see below), both LNR_A and LNR_AB migrate as a monomer at concentrations up to 100 μM, as judged by gel filtration chromatography.

Initial backbone assignments for ^{13}C, ^{15}N, and ^{1}H resonances were completed using the HNCA and HNCOCA experiments. Assignments were verified by the sequential assignment strategy using 150 ms three-dimensional (3D) ^{15}N-NOESY-HSQC, 200 ms two-dimensional (2D) ^{15}N-HSQC, and ^{13}C-HSQC. Data were taken at 25 °C on 1 mM ^{15}N-labeled or ^{15}N- and ^{13}C-labeled protein samples in 90% H_2O, 10% D_2O, and 10 mM $CaCl_2$ (pH 6.5). For side chain and NOE assignments used for structure calculations, ^{15}N and ^{1}H chemical shifts were also assigned for spectra recorded at 4 °C on the same samples, as well as for spectra recorded at 10 °C on a 1.5 mM ^{15}N-labeled protein sample in 50 mM deuterated PIPES, 10 mM $CaCl_2$, and 10% D_2O (pH 7.0). ^{1}H chemical shifts were directly calibrated using 2,2-dimethyl-2-silapeptane-5-sulfonate (DSS) as an internal standard, and ^{15}N and ^{13}C chemical shifts were referenced indirectly to DSS. Side chain assignments were determined from ^{15}N-TOCSY-HSQC (mixing time of 60 ms) combined with additional 2D experiments, including 2QF-COSY and 2D TOCSY (in both H_2O and D_2O, with mixing times ranging from 10 to 70 ms). 2D NOESY (mixing times of 175 and 200 ms) and ^{15}N-NOESY-HSQC (mixing time of 175 ms) experiments were used to obtain the spectra for the NOE assignments. Assignments were performed manually in NMRView. Ambiguities were resolved by cross validation from peaks observed in different NOE experiments (both homonuclear and heteronuclear experiments carried out at different temperatures and pH values). The legitimacy of the manual assignments was again cross validated with the fully automated assignment protocol in CYANA; only unambiguous NOE assignments were used in initial structure calculations. Once clear structural convergence was achieved, the preliminary structures were used to guide resolution of other ambiguities. Several iterations of this cycle of assignment followed by structure calculation were carried out until no further distinction among possibilities could be achieved. The final input to the CNS structure calculation protocol included 27 ambiguous constraints (among a total of 732), most of which were intraresidue ambiguities about side chain atom identity.

Dihedral angle restraints for the backbone ϕ angles were derived mainly from vicinal coupling constants ($^3J_{HNH_\alpha}$) determined from HNHA and HMQC-J experiments. TALOS (*19*) backbone angle predictions (with $\geq$80% consistency) were used to provide additional ϕ and ψ angle restraints. χ_1 angle restraints and stereospecific assignments for the β-protons were obtained using a combination of HNHB and short mixing time TOCSY (10 ms) and NOESY (50 ms) experiments. Stereospecific assignments for the NH_2 groups of asparagine and glutamine residues were determined on the basis of characteristic NOE patterns in a short mixing time NOESY spectrum (50 ms) and the chemical shift index (CSI).

NOE-derived distance constraints were obtained by stratifying the measured volumes of NOESY cross-peaks into five classes. Peaks from each class (1−5) were assigned a lower limit of 1.8 Å and an upper limit of 3.0, 3.5, 4.2, 4.8, and 5.5 Å, respectively. An additional 0.5 Å was added to the upper limit of stereochemically ambiguous NOEs. Specific volume cutoffs used for individual spectra were chosen to maximize agreement in class assignment for peaks seen in different spectra. Three disulfide-bond constraints were added on the basis of the previously established disulfide connectivity (*13*), verified by the observed NOEs.

Fifty preliminary structures that did not contain a Ca^{2+} ion were calculated using the torsion angle protocol in CNS (*20*) and then used as an input for the dynamic simulated annealing regularization and refinement (DGSA) protocol in CNS. The DGSA protocol was carried out in 30 000 steps starting from 3000 K using a new extended template molecule that contained an arbitrarily placed Ca^{2+} ion and three additional distance constraints from the predicted heavy atom donors to the Ca^{2+} ion (with an upper limit of 2.8 Å). DGSA runs with and without inclusion of the Ca^{2+} ion yielded essentially identical structural ensembles for the protein. Forty-eight of the 50 calculated structures contained no distance constraint violations greater than 0.3 Å and no dihedral angle constraint violations greater than 5° (Table 1). The 15 lowest-energy structures with Ca^{2+} were then chosen to calculate a minimized average structure, which was subjected to protein structure validation using PROCHECK-NMR (*21*). Structures were analyzed and visualized using the molecular graphics programs MOLMOL (*22*), GRASP (*23*), and POV-Ray 3.5 [POV-Ray Team (http://www.povray.org)]. Coordinates for the 15 lowest energy LNR_A structures and the energy-minimized mean structure have been deposited in the protein data bank under the accession code 1PB5.

RESULTS

Ca^{2+} Binding Affinity of LNR_A. We showed previously that folding of LNR_A to a unique disulfide isomer readily occurs in the presence, but not in the absence, of calcium (*13*). Indeed, the HSQC spectrum of LNR_A exhibits good chemical shift dispersion in the presence of excess Ca^{2+}, giving a single set of resonances indicative of a unique, well-defined structure. To evaluate the ion specificity of this binding site, we acquired one-dimensional (1D) NMR spectra of LNR_A in the presence of saturating concentrations of Zn^{2+}, Ni^{2+}, Mn^{2+} Cd^{2+}, and Mg^{2+}, and compared them with the spectra acquired in the presence or absence of Ca^{2+}. Spectra of LNR_A acquired in the presence of Zn^{2+}, Ni^{2+}, Mn^{2+}, and Mg^{2+} were all dominated by broad peaks and exhibited meager chemical shift dispersion; even the Cd^{2+} spectra only displayed a slight improvement in dispersion. These findings indicate that the LNR_A ion-binding site is highly selective for Ca^{2+} and does not readily accommodate other divalent metals.

We quantified the Ca^{2+} binding affinity of LNR_A by isothermal titration calorimetry (ITC). The module binds Ca^{2+}, with a dissociation constant of 40 ± 1 μM and with a stoichiometry of 1:1 (Figure 2). Plotting the chemical shifts of well-resolved resonances in a series of 1D and 2D NMR spectra in Ca^{2+} titration experiments gives a similar value of K_d (data not shown).

Table 1: NMR Restraints and Structural Statistics

Distance Restraints	
total	732
intraresidue	247
sequential ($\|i-j\|=1$)	202
medium-range ($2 \geq \|i-j\| \leq 4$)	179
long-range ($\|i-j\|>4$)	101
Ca^{2+} distances[a]	3
Dihedral Restraints	
total	52
ϕ ($C'_{i-1}-N_i-C_{\alpha i}-C'_i$)	24
ψ ($N_i-C_{\alpha i}-C'_i-N_{i+1}$)	17
χ_1 ($N_i-C_{\alpha i}-C_{\beta i}-C_{\gamma i}$)	11
Stereospecific Assignments	
total	
β-methylene groups	15
NH_2-terminal amide groups for Asn/Gln	4

Ramachandran Plot[b,c]

	total no. of residues	%
most favorable region	243 (17)	57.9
additionally allowed region	162 (10)	38.6
generously allowed region	0 (0)	0.0
disallowed region	15 (1)	3.6
glycine residues	60 (4)	
proline residues	15 (1)	
end residues	30 (2)	

Average rms Deviation	
experimental distance restraints (Å)	0.0393 ± 0.0001
experimental dihedral angle restraints (deg)	0.6662 ± 0.0158
idealized covalent geometry	
bonds (Å)	0.0049 ± 0.0001
angles (deg)	0.5942 ± 0.0051
impropers (deg)	0.3411 ± 0.0038

Average rms Deviation of Atomic Coordinates among the 15 Structures

	all residues	residues 4−34
backbone (Å)	0.270	0.114
heavy atoms (Å)	0.717	0.490

[a] Distance constraints from side chain oxygens of N15, D30, and D33 to Ca^{2+} as described in Materials and Methods. [b] Region of the Ramachandran plot as defined by PROCHECK-NMR. [c] Values in parentheses are for the minimized average structure of the 15 lowest-energy structures.

NMR Structure Determination. We determined the three-dimensional structure of LNR_A by solution NMR spectroscopy. Assignments and constraints for NMR structure calculations were derived from spectra of samples containing 10 mM Ca^{2+} at pH 7.0, because saturating Ca^{2+} concentrations and neutral pH are critical for maintaining a well-folded structure (see above). Constraints used for structure calculations and statistics for the 15 lowest-energy structures and their minimized average are summarized in Table 1. PROCHECK-NMR evaluation of the ensemble and the minimized average structure indicate good overall stereochemical geometry with only the first cysteine residue (Cys4) in a disallowed region of the Ramachandran plot.

Description of the Structure. LNR_A adopts a single conformation in solution, with well-defined backbone coordinates between its first and last cysteines. Superposition of the ensemble of structures (Figure 3A) yields a root-mean-square deviation from the minimized average structure of 0.11 Å for the backbone atoms and 0.49 Å for all heavy atoms (residues C4−C34, Table 1).

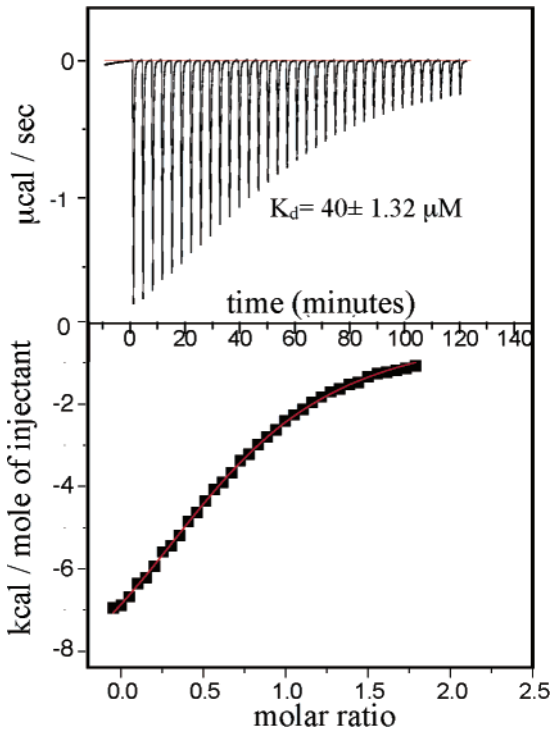

FIGURE 2: Affinity of LNR_A for Ca^{2+} determined by isothermal titration calorimetry (ITC). The heat absorbed by LNR_A is plotted as a function of the amount of added Ca^{2+}. LNR_A binds Ca^{2+} in a 1:1 stoichiometry with a K_d of 40 ± 1.3 mM.

Structures calculated without Ca^{2+} constraints contain an empty space that is large enough to accommodate a Ca^{2+} ion, surrounded by the side chains of conserved acidic and polar residues predicted to participate in Ca^{2+} coordination (*13*). The β-protons of these side chains, which belong to N15, D30, and D33, exhibit significant deviations from random coil chemical shifts, consistent with their participation in coordinating Ca^{2+}. On the basis of sequence alignment, the previous observation that mutation of each of these residues to alanine abrogates proper folding (*13*), and the observed hole in the structure calculated without inclusion of a calcium ion, we inferred that the calcium ion occupies the empty space surrounded by these side chains. Therefore, we included three explicit distance constraints (with an upper limit of 2.8 Å) from a Ca^{2+} ion to the side chain oxygens of N15, D30, and D33 during final refinement in CNS. These additional constraints did not result in any new NOE or angle violations, and the rmsd between the minimized average of the 15 lowest-energy structures calculated with and without the Ca^{2+} constraints is 0.12 Å.

LNR_A is held together primarily by its three disulfide bonds and by participation of N15, D30, and D33 in coordinating the bound Ca^{2+} ion (Figure 3B). The module contains little secondary structure, possessing just a short α-helical turn from C9 to D12 and a 3-10-helix between W29 and D33. Surprisingly, the hydrophobic side chains of V17, L20, H25, and W29 are not buried within the central core of the module. Instead, the core is constructed from C9 and C22, which form a disulfide bond, the side chains of A13, S19, N23, and A26, and the calcium-coordinating residues

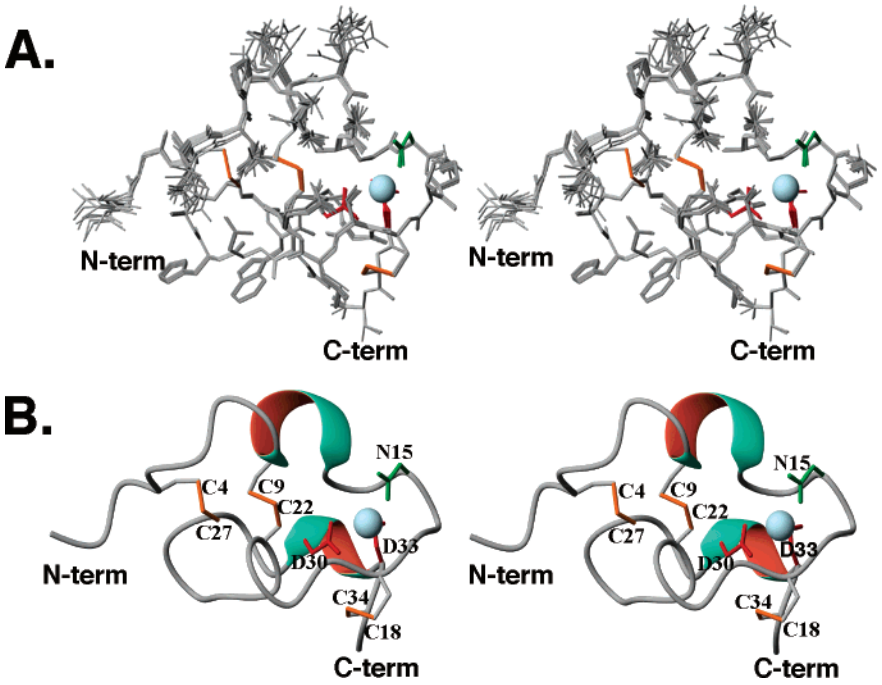

FIGURE 3: NMR solution structure of LNR_A. (A) Stereoview of the 15 lowest-energy structures of LNR_A. The best-fit superposition of the polypeptide backbone between the first and last cysteine residues is shown. The three disulfide bonds are orange; the Ca^{2+} ion is blue, and the Ca^{2+}-coordinating residues are red (D30/D33) and green (N15). (B) Stereoview of the ribbon diagram for the minimized average structure of LNR_A.

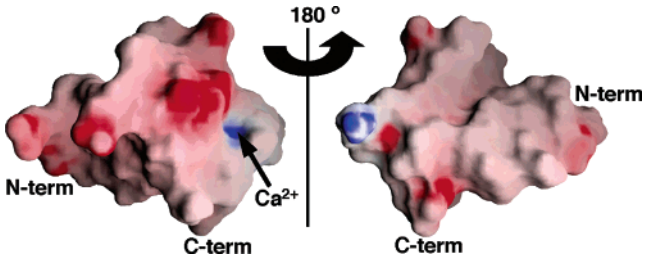

FIGURE 4: Surface representation of LNR_A, colored according to electrostatic potential. The surface has been colored using a sliding scale from blue (20 kT/e) to red (−20 kT/e). In the left panel, the module is oriented as in Figure 3.

D30 and D33, which have solvent-accessible surface areas of 0 and 21 $Å^2$ (14%), respectively. The backbone amide protons of V17, C22, C27, and W29 exhibit protection against exchange even after 3 h at pH 7.0, indicating that the core is reasonably well-packed despite the paucity of secondary structure. In the absence of calcium, the module would bear a highly negative net charge. However, the bound calcium ion attenuates the charge of the buried side chains of D30 and D33 at the surface (Figure 4).

Interaction Face between the First Two LNR Modules. We examined the structural influence of LNR_A and LNR_B upon each other by comparing ^{15}N,^{1}H-HSQC spectra of LNR_A, LNR_B, and the LNR_AB module pair in a chemical shift perturbation experiment (Figure 5). Not surprisingly, the perturbed region includes residues at the C-terminal end of LNR_A around the covalent connection between modules. More significantly, however, the influence of intermodule interactions between LNR_A and LNR_B extends further, along the face of LNR_A that in isolation exposes the side chains of three hydrophobic residues, L20, H25, and W29 (Figure 5).

DISCUSSION

Notch proteins such as human Notch1 have a modular organization in which different types of repeated structural units combine to form the mature, functional receptor. The extracellular subunit of human Notch1 contains 36 EGF-like repeats and three LNR modules, while the NTM subunit contains a series of seven ankyrin repeats. Functions have been ascribed to the EGF modules and the ankyrin repeats: the EGF-like modules encompass the binding site(s) for ligands of the Delta and Serrate families (*24*), and the ankyrin repeats participate in the formation of the nuclear transcriptional activation complex (*25*−*27*). The three LNR modules, which are present in all Notch receptors and unique to them, are cysteine-rich repeats located near the C-terminal end of the NEC subunit. Though the details of their mechanistic role have not been fully elucidated, these repeats participate in maintaining the mature Notch heterodimer in a resting state prior to ligand-induced activation (*27*).

The structure of the prototype LNR module reported here represents a new fold within the general class of irregular, disulfide-bonded structures (*28*). Despite the lack of appreciable secondary structure, the unique arrangement of three disulfide bonds and a single Ca^{2+} ion is sufficient to hold the module in a well-defined, compact tertiary structure. Among cysteine-rich extracellular modules, LNR_A shares the unusual property of having a structurally important Ca^{2+}-binding site with the ligand-binding, type A (LA) modules of the LDL receptor (*29*, *30*), and a subset of Ca^{2+}-binding EGF-like (cbEGF) modules (*31*). However, the detailed features of the LNR_A Ca^{2+} coordination site, which is established in part by the two aspartates of the DGGD sequence from residues 30−33 and the conserved N15, are different from the arrangements seen in LA and cbEGF modules. With regard to Ca^{2+} coordination, it is also worth noting that the serine residue at position 19 of the human

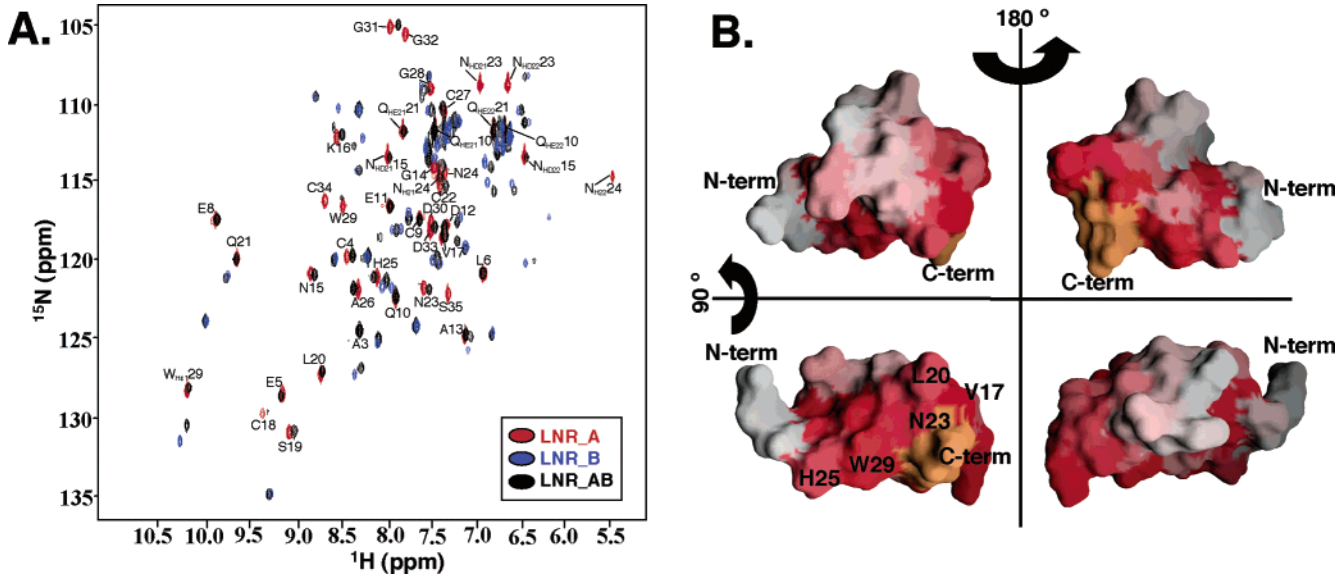

FIGURE 5: Interdomain interactions between LNR_A and LNR_B. (A) Comparison of assigned ^{15}N−^{1}H HSQC spectra of LNR_A (red), LNR_B (blue), and the LNR_AB pair (black) in an overlay plot. (B) Molecular surface representation of LNR_A colored according to chemical shift perturbation. The perturbation scale was established by calculating the sum of HN and ^{15}N chemical shift differences between resonances of LNR_A in the isolated module (LNR_A) and in the module pair (LNR_AB). In the top left panel, the module is oriented as in Figure 3.

Notch1 LNR_A structure is commonly an aspartate or an asparagine in other LNR modules (Figure 1B). Introduction of an additional constraint between the side chain oxygen of S19 and the Ca^{2+} ion does not result in any new violations during structure calculations. Thus, it is certainly possible that S19 of LNR_A (and by extension the corresponding aspartate or asparagine residues of other LNR modules) is also part of the Ca^{2+} coordination sphere. Indeed, LNR_B, which has an aspartate residue at this position, binds Ca^{2+} ~4-fold more tightly than LNR_A, an increase in affinity consistent with what one might expect if participation of an aspartate residue in binding creates a more well-optimized Ca^{2+} coordination site. Finally, the modest Ca^{2+} affinity of LNR modules suggests the possibility that the Ca^{2+} coordination sphere is not fully occupied, and that a bridging ligand at the open coordination site might participate in stabilizing intra- or intermolecular interactions of one or all of the LNR modules.

Several lines of evidence suggest that the three Notch LNRs are structurally interdependent, with the linker regions defining a precise intermodule arrangement required for negative regulation. First, the Notch LNRs are always found as a group of three adjacent modules separated from each other by two 6−10-residue linkers. Second, the high degree of conservation among the LNR modules from different species also extends to the linker sequences between them (Figure 1). Third, an arginine to tryptophan (R672Y) gain-of-function mutation in the worm LIN-12 protein (*14*) lies in the linker between LNR_A and LNR_B, suggesting that the native sequence of this linker is required to keep the receptor in its resting conformation.

To determine whether LNR_A is structurally influenced by the presence of the neighboring LNR_B module and/or the A−B linker, we compared the HSQC spectra of the individual LNR_A and LNR_B modules with that of the LNR_AB module pair. Upon covalent connection to LNR_B *via* the native linker, the amides of LNR_A residues that exhibit perturbations lie clustered on one face of the module. These residues include not only the C-terminal residues of LNR_A but also exposed hydrophobic residues V17, L20, H25, A26, and W29 and the side chain amides of N23. The involvement in intermodule interactions with LNR_B likely explains why these hydrophobic residues (especially W29, which is highly conserved) are exposed on the module surface, rather than buried in its interior.

Although there is functional evidence that the LNRs are critical for the regulation of Notch signaling, the details of how they maintain the receptor in a resting conformation prior to ligand binding and prevent the activating intracellular cleavage remain unknown. A major unresolved mechanistic question is how the binding of a ligand to the N-terminal modules of the Notch NEC subunit hundreds of angstroms from the cell membrane triggers proteolytic cleavage of the noncovalently associated NTM subunit within 12 residues of the membrane-spanning sequence (*32*, *33*). One proposed model for how ligand binding triggers activation is the "mechanical tug" model, which supposes that binding of cell surface Notch receptors to ligand-bearing cells exerts a force on the NEC subunit that leads to heterodimer dissociation or exposure of the S2 cleavage site (*34*, *35*). Tight packing of the LNR interdomain interfaces might be critical for maintaining Notch in its resting conformation, or for use in propagating the "tug" (signal) from the amino-terminal ligand-binding EGF modules to expose the S2 cleavage site within NTM. Alternatively, the Notch NEC subunit might undergo a dramatic conformational rearrangement in response to ligand, analogous to the large-scale structural reorganizations proposed for integrins in response to ligand (*36*−*38*), or lipoprotein receptors in response to changes in pH (*39*). Ultimately, a comprehensive view of how ligand binding leads to activation will require an understanding of how both adjacent and distantly positioned extracellular modules of Notch are structurally and functionally integrated with one another.

ACKNOWLEDGMENT

We are indebted to Dr. Gerhard Wagner for use of NMR spectrometers at Harvard Medical School, Dr. C. James McKnight for use of NMR facilities at the Boston University School of Medicine (Boston, MA), and Dr. Natalia Beglova for assistance with preliminary NMR spectra of LNR_B and the LNR_AB pair.

REFERENCES

1. Greenwald, I. (1998) *Genes Dev. 12*, 1751−1762.
2. Allman, D., Punt, J. A., Izon, D. J., Aster, J. C., and Pear, W. S. (2002) *Cell 109* (Suppl.), S1−S11.
3. Ellisen, L. W., Bird, J., West, D. C., Soreng, A. L., Reynolds, T. C., Smith, S. D., and Sklar, J. (1991) *Cell 66*, 649−661.
4. Pear, W. S., Aster, J. C., Scott, M. L., Hasserjian, R. P., Soffer, B., Sklar, J., and Baltimore, D. (1996) *J. Exp. Med. 183*, 2283−2291.
5. Aster, J. C., Xu, L., Karnell, F. G., Patriub, V., Pui, J. C., and Pear, W. S. (2000) *Mol. Cell. Biol. 20*, 7505−7515.
6. Brown, M. S., Ye, J., Rawson, R. B., and Goldstein, J. L. (2000) *Cell 100*, 391−398.
7. Yu, G., Nishimura, M., Arawaka, S., Levitan, D., Zhang, L., Tandon, A., Song, Y. Q., Rogaeva, E., Chen, F., Kawarai, T., Supala, A., Levesque, L., Yu, H., Yang, D. S., Holmes, E., Milman, P., Liang, Y., Zhang, D. M., Xu, D. H., Sato, C., Rogaev, E., Smith, M., Janus, C., Zhang, Y., Aebersold, R., Farrer, L. S., Sorbi, S., Bruni, A., Fraser, P., and St George-Hyslop, P. (2000) *Nature 407*, 48−54.
8. Chung, H. M., and Struhl, G. (2001) *Nat. Cell Biol. 3*, 1129−1132.
9. Esler, W. P., Kimberly, W. T., Ostaszewski, B. L., Ye, W., Diehl, T. S., Selkoe, D. J., and Wolfe, M. S. (2002) *Proc. Natl. Acad. Sci. U.S.A. 99*, 2720−2725.
10. Hu, Y., Ye, Y., and Fortini, M. E. (2002) *Dev. Cell 2*, 69−78.
11. Artavanis-Tsakonas, S., Rand, M. D., and Lake, R. J. (1999) *Science 284*, 770−776.
12. Nam, Y., Aster, J. C., and Blacklow, S. C. (2002) *Curr. Opin. Chem. Biol. 6*, 501−509.
13. Aster, J. C., Simms, W. B., Zavala-Ruiz, Z., Patriub, V., North, C. L., and Blacklow, S. C. (1999) *Biochemistry 38*, 4736−4742.
14. Greenwald, I., and Seydoux, G. (1990) *Nature 346*, 197−199.
15. Rand, M. D., Grimm, L. M., Artavanis-Tsakonas, S., Patriub, V., Blacklow, S. C., Sklar, J., and Aster, J. C. (2000) *Mol. Cell. Biol. 20*, 1825−1835.
16. Cavanagh, J., Fairbrother, W. J., Palmer, A. G., III, and Skelton, N. J. (1996) *Protein NMR Spectroscopy*, Academic Press, San Diego.
17. Delaglio, F., Grzesiek, G., Vuister, G., Pfeifer, J., and Bax, A. (1995) *J. Biomol. NMR 6*, 227−293.
18. Johnson, B., and Blevins, R. (1994) *J. Biomol. NMR 4*, 603−614.
19. Cornilescu, G., Delaglio, F., and Bax, A. (1999) *J. Biomol. NMR 13*, 289−302.
20. Brunger, A. T., Adams, P. D., Clore, G. M., DeLano, W. L., Gros, P., Grosse-Kunstleve, R. W., Jiang, J. S., Kuszewski, J., Nilges, M., Pannu, N. S., Read, R. J., Rice, L. M., Simonson, T., and Warren, G. L. (1998) *Acta Crystallogr. D54*, 905−921.
21. Laskowski, R. A., Rullmann, J. A. C., MacArthur, M. W., Kaptein, R., and Thornton, J. M. (1996) *J. Biomol. NMR 8*, 477−486.
22. Koradi, R., Billeter, M., and Wüthrich, K. (1996) *J. Mol. Graphics 14*, 51−55.
23. Nicholls, A., Sharp, K., and Honig, B. (1991) *Proteins: Struct., Funct., Genet. 11*, 281−296.
24. Rebay, I., Fleming, R. J., Fehon, R. G., Cherbas, L., Cherbas, P., and Artavanis-Tsakonas, S. (1991) *Cell 67*, 687−699.
25. Fortini, M. E., and Artavanis-Tsakonas, S. (1994) *Cell 79*, 273−282.
26. Roehl, H., Bosenberg, M., Blelloch, R., and Kimble, J. (1996) *EMBO J. 15*, 7002−7012.
27. Struhl, G., and Adachi, A. (1998) *Cell 93*, 649−660.
28. Orengo, C. A., Michie, A. D., Jones, S., Jones, D. T., Swindells, M. B., and Thornton, J. M. (1997) *Structure 5*, 1093−1108.
29. Blacklow, S. C., and Kim, P. S. (1996) *Nat. Struct. Biol. 3*, 758−762.
30. Fass, D., Blacklow, S., Kim, P. S., and Berger, J. M. (1997) *Nature 388*, 691−693.
31. Downing, A. K., Knott, V., Werner, J. M., Cardy, C. M., Campbell, I. D., and Handford, P. A. (1996) *Cell 85*, 597−605.
32. Mumm, J. S., Schroeter, E. H., Saxena, M. T., Griesemer, A., Tian, X., Pan, D. J., Ray, W. J., and Kopan, R. (2000) *Mol. Cell 5*, 197−206.
33. Brou, C., Logeat, F., Gupta, N., Bessia, C., LeBail, O., Doedens, J. R., Cumano, A., Roux, P., Black, R. A., and Israel, A. (2000) *Mol. Cell 5*, 207−216.
34. Parks, A. L., Klueg, K. M., Stout, J. R., and Muskavitch, M. A. (2000) *Development 127*, 1373−1385.
35. Di Fiore, P. P., and De Camilli, P. (2001) *Cell 106*, 1−4.
36. Beglova, N., Blacklow, S. C., Takagi, J., and Springer, T. A. (2002) *Nat. Struct. Biol. 9*, 282−287.
37. Takagi, J., Petre, B. M., Walz, T., and Springer, T. A. (2002) *Cell 110*, 599−611.
38. Shimaoka, M., Takagi, J., and Springer, T. A. (2002) *Annu. Rev. Biophys. Biomol. Struct. 31*, 485−516.
39. Rudenko, G., Henry, L., Henderson, K., Ichtchenko, K., Brown, M. S., Goldstein, J. L., and Deisenhofer, J. (2002) *Science 298*, 2353−2358.

BI034156Y